Volume 59
Number 53
7 July 2023
Pages 8149–8312

ChemComm

Chemical Communications

rsc.li/chemcomm

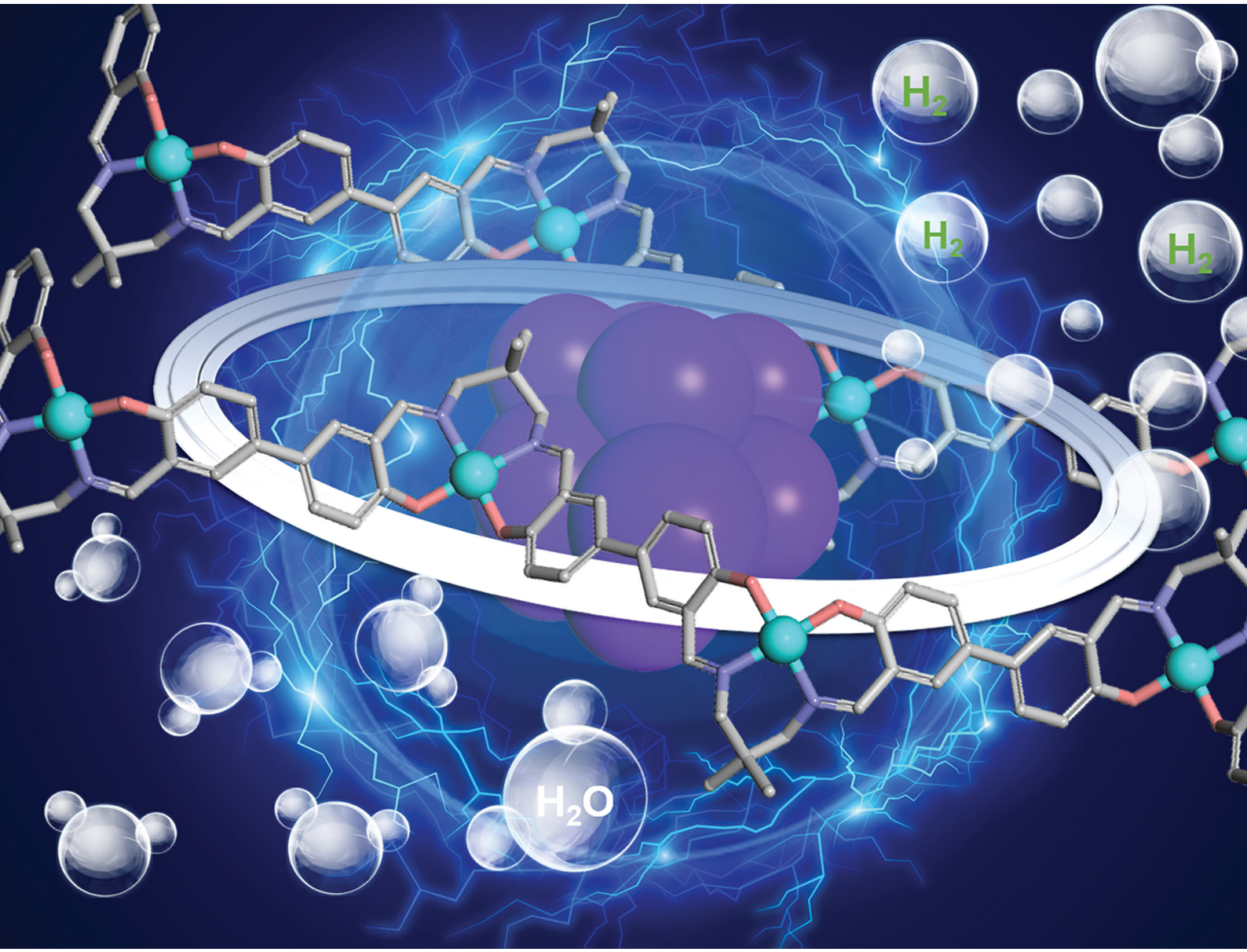

ISSN 1359-7345

ROYAL SOCIETY OF CHEMISTRY

COMMUNICATION

Wenjie Shi, Dichang Zhong, Tong-Bu Lu *et al.*
A cobalt metalized polymer modulates the electronic structure of Pt nanoparticles to accelerate water dissociation kinetics

ChemComm

COMMUNICATION

View Article Online
View Journal | View Issue

Cite this: *Chem. Commun.*, 2023, 59, 8222

Received 29th April 2023,
Accepted 6th June 2023

DOI: 10.1039/d3cc02082g

rsc.li/chemcomm

A cobalt metalized polymer modulates the electronic structure of Pt nanoparticles to accelerate water dissociation kinetics†

Xiaomei Hu,[a] Weixue Tao,[a] Wenjie Shi, *[ab] Dichang Zhong*[a] and Tong-Bu Lu *[a]

Herein, we construct a composite material of Pt-NPs@NPCNs–Co by anchoring Pt nanoparticles (Pt NPs) and Co-salen covalent organic polymer (Co-COP) onto N, P co-doped carbon nanotubes (NPCNs), thereby offering an integrated approach to enhance H_2O dissociation. The bimetallic catalyst Pt-NPs@NPCNs–Co demonstrates exceptional HER performance, and the overpotential at 40 mA cm^{-2} is lower than that of 20% Pt/C. When the overpotential is 50 mV, the mass activity of Pt-NPs@NPCNs–Co is 2.8 times that of the commercial Pt/C catalyst. Experimental results reveal that the synergistic interplay between Pt NPs and Co contributes to the excellent electrocatalytic performance observed. Density function theory calculations found that Co effectively modulates the electronic structure of Pt NPs and lowers the activation energy of the Volmer step, thereby accelerating the water dissociation kinetics of Pt NPs. This research contributes to the advancement of knowledge regarding the development of more efficient bimetallic co-catalytic electrocatalysts in alkaline media.

The hydrogen evolution reaction (HER) activity of Pt-based catalysts under alkaline conditions is approximately two orders of magnitude lower than that under acidic conditions due to the high activation barrier of H_2O dissociation (Volmer step: $H_2O + e^- \rightarrow H^* + OH^-$).[1,2] To address this challenge, extensive efforts have been made to develop efficient and stable electrocatalysts.[3–8] The introduction of a second metal component into Pt-based catalysts has been found to enhance the HER activity.[9–13] For instance, Markovic *et al.*[14] to used $Ni(OH)_2$ clusters on Pt electrodes speed up water dissociation and hydrogen intermediate generation, while Yan *et al.*[15] used oxygen-rich MgO nanosheets to create an acid-like environment, improving the HER kinetics of Pt NPs and reducing the overpotential. These studies point to a brand-new strategy for boosting the performance of Pt-based catalysts in alkaline conditions.

Understanding the interaction between non-platinum co-catalysts and platinum in HER is vital, especially when the added metal alters the interfacial structure. Unveiling this could improve HER performance by leveraging charge polarization or swift electron transport in dual-component materials.[10,12] A more in-depth consideration of the synergistic mechanism for the assembled components should be given, particularly with regard to specific coordination structures.[16,17] One-dimensional (1D) polymer structures in coordination chemistry have gained interest for their ability to elucidate the role of non-platinum atomic co-catalysts.[18] When stacked orderly, they provide more exposed edge sites, enhancing substance transport and enabling the study of synergistic mechanisms.[19–23]

In this work, we introduce a hybrid platinum-based catalyst, called Pt-NPs@NPCNs–Co, aimed at improving HER activity and catalyst stability. The three-step synthesis process combines a platinum-bimetallic system with carbon nanotubes (CNTs). Small Pt NPs (about 3 nm) are evenly distributed on the NPCNs–Co surface, primarily exposing the (111) face. The Pt-NPs@NPCNs–Co shows better HER performance in a 1 M KOH solution than 20% Pt/C, with a lower overpotential at 40 mA cm^{-2}. The mass activity at 50 mV overpotential is 2.8 times higher than that of commercial Pt/C catalysts. This research offers valuable insights for creating efficient platinum-bimetallic systems for the alkaline HER.

The Pt-NPs@NPCNs–Co composite preparation is outlined in Scheme 1. Initially, the NPCN precursor is produced by mixing melamine and phosphoric acid, which interact with the carboxyl group (–COOH) of functionalized carbon nanotubes *via* hydrogen bonding.[24] A Schiff base reaction was carried out to adhere the Co-COP to the surface of the NPCNs, which yielded the intermediate NPCNs–Co. Thereafter, we synthesized Pt-NPs@NPCNs–Co using thermal reduction to deposit Pt NPs on the NPCNs–Co. As shown in Fig. 1a, the main diffraction peaks of NPCNs were maintained

[a] *Institute for New Energy Materials & Low Carbon Technologies, School of Material Science & Engineering, School of Chemistry & Chemical Engineering, Tianjin University of Technology, Tianjin 300384, China. E-mail: wjshi@email.tjut.edu.cn, dczhong@email.tjut.edu.cn, lutongbu@tjut.edu.cn*

[b] *Guangdong Provincial Key Laboratory of Fuel Cell Technology, Guangdong, China*

† Electronic supplementary information (ESI) available. See DOI: https://doi.org/10.1039/d3cc02082g

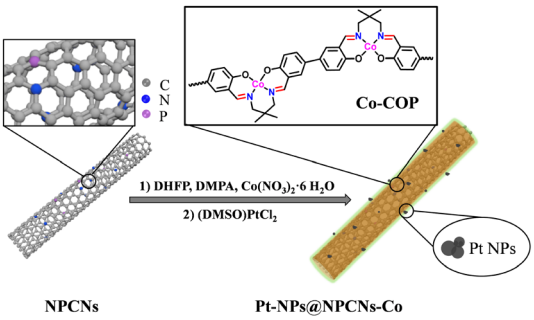

Scheme 1 The synthetic procedure of Pt-NPs@NPCNs–Co.

in NPCNs–Co, Pt-NPs@NPCNs and Pt-NPs@NPCNs–Co, proving that the structure underwent no changes during the preparation process. The diffraction peaks at 39.8°, 46.3° and 67.5° belong to the (111), (200) and (220) planes of Pt NPs (PDF: No. 04-0802), indicating that Pt NPs were successfully anchored to the surface of the NPCNs–Co.[3,25] The Fourier transform infrared spectroscopy (FT-IR) spectrum of Pt-NPs@NPCNs–Co (Fig. 1b) shows a characteristic absorption peak at around 1625 cm^{-1}, which corresponds to the C=N stretching vibration band.[26] The absence of the characteristic C=O stretching vibration band at 1660 cm^{-1} of 4,4′-dihydroxy-3,3′-diformylbiphenyl (DHFP) further proved that DHFP and 2,2-dimethyl-1,3-propanediamine were successful polycondensated.

The transmission electron microscopy (TEM) image of the NPCNs–Co showed a thin layer of Co-COP adhered to the surface of NPCNS (Fig. S1, ESI†). The high-resolution TEM (HRTEM) image displayed that Pt NPs with an average size of 3 nm are uniformly distributed on the NPCNs–Co and NPCNS (Fig. 1e, f and Fig. S2, ESI†). The averaged lattice spacings of Pt NPs were 0.22 nm, which is consistent with the lattice plane (111) of the face-centered-cubic (fcc) phase of Pt.[27] The content of Pt in Pt-NPs@NPCNs–Co and Pt-NPs@NPCNs was detected by inductively coupled plasma mass spectrometry (ICP-MS). The results showed approximately 3.25% and 4.23% of Pt in Pt-NPs@NPCNs–Co and Pt-NPs@NPCNs, respectively (Table S1, ESI†). Furthermore, elemental mapping by energy-dispersive X-ray spectroscopy (EDS) revealed the homogenous dispersion of Pt, Co, and P on the Pt-NPs@NPCNs–Co (Fig. S3, ESI†). In order to verify the value of Pt and Co in Pt-NPs@NPCNs–Co, X-ray photoelectron spectroscopy (XPS) analysis was performed to probe the near-surface elemental composition and the chemical states. The high-resolution Pt 4f XPS spectrum of Pt-NPs@NPCNs–Co reveals two peaks, Pt $4f_{7/2}$ and Pt $4f_{5/2}$ which can be deconvoluted into two peaks (Fig. 1c). Binding energies of 71.6 and 74.8 eV are assigned to Pt $4f_{7/2}$ and Pt $4f_{5/2}$ of Pt-NPs@NPCNs–Co and Pt-NPs@NPCNs, which are ascribed to Pt^0 in Pt NPs. In addition, peaks at a binding energy of about 73.3 eV and 76.6 eV were attributed to Pt^{2+} species, which were a result of single Pt atoms linked to the N and C atoms.[4] The peaks of Pt^0 species in Pt-NPs@NPCNs–Co were negatively shifted 0.1 eV when compared to those in Pt-NPs@NPCNs, confirming electronic interaction by charge transfer from the NPCNs–Co substrate to the Pt sites, which leads to high HER performance.[5,28] The peak-fitting analysis of the Co 2p XPS spectra of Pt-NPs@NPCNs–Co and NPCNs–Co is shown in Fig. 1d. The peaks of 781.6 and 796.5 eV are attributed to the binding energy of Co $2p_{3/2}$ and Co $2p_{1/2}$ of Co^{2+}, respectively. Besides, there are two satellite peaks of Co $2p_{3/2}$ and Co $2p_{1/2}$ of Co^{2+} at 785.8 and 803.4 eV.[29] Comparison with NPCNs–Co showed that the peak location of Co $2p_{3/2}$ and Co $2p_{1/2}$ in Pt-NPs@NPCNs–Co had shifted positively by 0.1 eV, which corresponded to the binding energy negative shift of Pt^0. This indicates the transfer of electrons from Co to Pt NPs in Pt-NPs@NPCNs–Co.

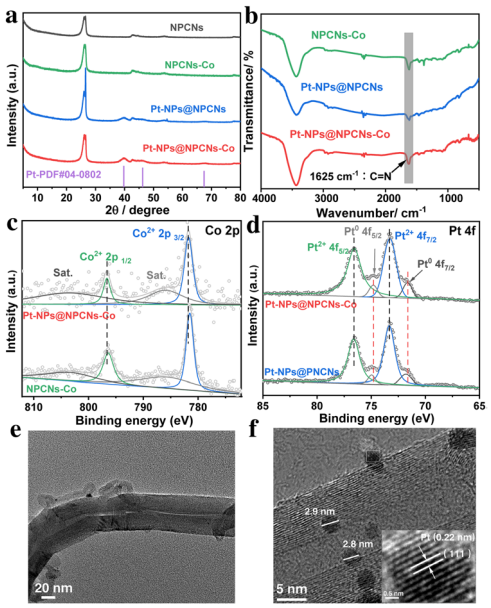

Fig. 1 (a) XRD spectra of Pt-NPs@NPCNs–Co, Pt-NPs@NPCNs, NPCNs–Co and pristine NPCNS. (b) FT-IR spectra of the corresponding samples of Pt-NPs@NPCNs–Co, Pt-NPs@NPCNs and NPCNs–Co. High-resolution XPS spectra of (c) Pt 4f, (d) Co 2p. (e) and (f) HRTEM image of Pt-NPs@NPCNs–Co.

In the N 1s XPS spectrum of Pt-NPs@NPCNs–Co shown in Fig. S4 (ESI†), the peaks at binding energies of 399.6, 400.4, 401.4 and 404.0 eV were ascribed to pyridinic N, pyrrolic N, graphitic N and oxidized N, respectively.[25] It is worth noting that the peak at 399.6 eV was assigned to pyridinic N, which confirmed that the N element was successfully doped into the carbon nanotube skeleton.[30] Furthermore, NPCNs–Co and Pt-NPs@NPCNs–Co displayed peaks at ~398.7 eV in their N 1s spectra (Fig. S5, ESI†), indicating the presence of Co–N coordination. In contrast, Pt-NPs@NPCNs did not exhibit such peaks (Fig. S6, ESI†), confirming the absence of Co–N coordination in that case. Hence, it was demonstrated that DHFP-Co polymerized successfully on the surface of NPCNS. As shown in Fig. S4 (ESI†), the deconvoluted O 1s XPS spectra of Pt-NPs@NPCNs–Co, displayed four peaks with binding energies of about 531.1, 531.8, 532.7 and 533.6 eV, corresponding to Co–O, C=O, C–OH and C–O, respectively.[31] Pt-NPs@NPCNs–Co showed excellent thermal stability (Fig. S7, ESI†) and had a similar surface area and pore size to Pt-NPs@NPCNs (Fig. S8, ESI†).

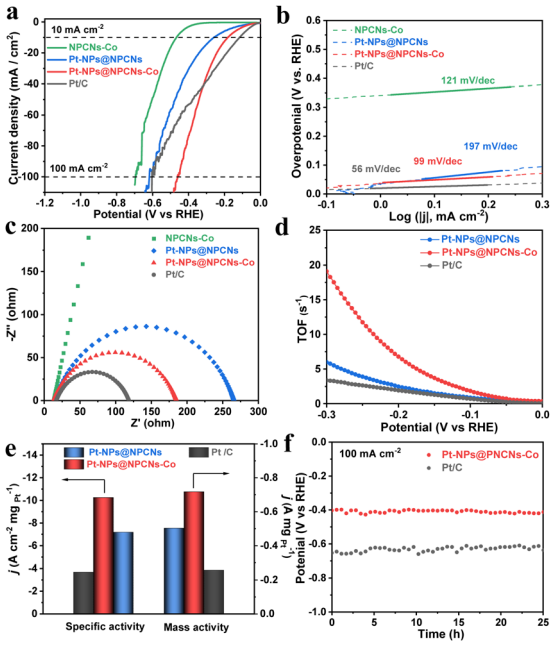

Fig. 2 Electrocatalytic HER activity characterization of the prepared samples. (a) LSV curves, (b) Tafel plots, (c) Nyquist plots, (d) TOF curves converted according to LSV, (e) specific activity and mass activity at an overpotential of 50 mV, (f) chronoamperometric curves of Pt-NPs@NPCNs–Co and 20% Pt/C at a current density of 100 mA cm^{-2}.

The HER performance of the catalysts was tested in an N_2-saturated 1.0 M KOH solution at room temperature, using a three-electrode setup with a glassy carbon electrode (GC) as the working electrode. Both single metal catalysts NPCNs–Co and Pt-NPs@NPCNs exhibited weak HER activity at current densities of 10 mA cm^{-2} with overpotential of 467 mV and 259 mV, respectively. In contrast, the introduction of Co into Pt-NPs@NPCNs significantly enhanced their HER activity, requiring only an overpotential of 182 mV to drive the same current density, which was lower than that of the single metal catalyst of NPCNs–Co and Pt-NPs@NPCNs. Commercial 20% Pt/C was also evaluated under the same conditions and the linear sweep voltammetry (LSV) curves (Fig. 2a) illustrated that it had superior HER activity at low potential, with an overpotential of 116 mV at 10 mA cm^{-2}, albeit higher than te previously reported value due to the loading mass of catalyst on GC being 0.057 mg cm^{-2}.[32] At 40 mA cm^{-2}, the HER activity of Pt-NPs@NPCNs–Co even exceeded that of commercial 20% Pt/C. These findings suggest that the coordination of Co within Pt-NPs@NPCNs–Co synergistically enhances their catalytic activity, contributing to the observed improvements in HER performance.

To further evaluate the HER kinetics and catalytic efficiency of the electrocatalysts, we plotted the Tafel slope analysis by linear fitting of the polarization curves. As shown in Fig. 2b, the Tafel slope measured for Pt-NPs@NPCNs–Co (99 mV dec^{-1}) is much lower compared to that of Pt-NPs@NPCNs (197 mV dec^{-1}) and NPCNs–Co (121 mV dec^{-1}) in 1 M KOH electrolyte, and slightly higher than the Tafel slope of the commercial 20% Pt/C (56 mV dec^{-1}). These results suggest that Pt-NPs@NPCNs–Co follows the Volmer–Heyrovsky mechanism for the HER. Moreover, the rate-determining step (RDS) was determined as the desorption of dissociated adsorbed hydrogen (H*) from the catalyst surface combined with an electron and water to form a hydrogen molecule (Cat-H* + H_2O + e^- → H_2 + OH^- + Cat). Notably, the RDS of NPCNs–Co and Pt-NPs@NPCNs is the Volmer step where H_2O dissociates into H* on the surface of the catalyst (H_2O + e^- + Cat → Cat-H* + OH^-). Therefore, these results confirm that Pt-NPs@NPCNs–Co possesses favorable catalytic kinetics towards the HER.[33–35]

The intrinsic HER activity of the electrocatalysts was investigated using electrochemical surface area (ECSA) analysis and electrochemical impedance spectroscopy (EIS). The C_{dl} values of Pt-NPs@NPCNs–Co were estimated to be 1.29 mF cm^{-2} (Fig. S9, ESI†), slightly larger than Pt-NPs@NPCNs (1.10 mF cm^{-2}) and NPCNs–Co (0.84 mF cm^{-2}), but lower than commercial 20% Pt/C (4.61 mF cm^{-2}), suggesting that Pt-NPs@NPCNs–Co has more exposed active sites than the other catalyst, except 20% Pt/C. EIS analysis revealed that Pt-NPs@NPCNs–Co has faster electron/proton transfer at the electrocatalyst/electrolyte interface, with a lower R_{ct} (172.5 Ω) than Pt-NPs@NPCNs (250.6 Ω) and NPCNs–Co (11681 Ω) (Fig. 2c and Table S2, ESI†). The turnover frequency (TOF) values were calculated assuming that all atomic sites are catalytically active.[36] As shown in Fig. 2d, the TOF of Pt-NPs@NPCNs–Co is one order of magnitude larger than the control catalysts, roughly 3 and 6 times higher than that of Pt-NPs@NPCNs and 20% Pt/C, respectively. Additionally, the specific activity and mass activity were calculated as important indices for estimating the HER catalytic performance of noble metals. As displayed in Fig. 2e, at an overpotential of 50 mV, the specific activities of Pt-NPs@NPCNs–Co, Pt-NPs@NPCNs and 20% Pt/C are 10.3, 7.2 and 3.7 A cm^{-2} mg_{Pt}^{-1}, respectively. It was also observed that the Pt-NPs@NPCNs–Co catalyst has a higher mass activity than Pt-NPs@NPCNs and 20% Pt/C; the mass activities of Pt-NPs@NPCNs–Co, Pt-NPs@NPCNs and 20% Pt/C are 0.72, 0.50 and 0.26 A mg_{Pt}^{-1}, respectively. These results suggest that the Pt-NPs@NPCNs–Co has higher Pt utilization than commercial 20% Pt/C. Electrocatalytic stability is another criterion for evaluating an electrocatalyst. According to Fig. S10 (ESI†) and Fig. 2f, the cyclic voltammetry (CV) and chronopotentiometry tests indicated that Pt-NPs@NPCNs–Co displayed the best long term durability and higher HER activity than the other catalysts. The LSV curve of Pt-NPs@NPCNs–Co displayed a negative shift after 3000 cycles compared with the initial curve in 1.0 M KOH. The chronopotentiometry test of the Pt-NPs@NPCNs–Co remains nearly unchanged after 25 h conducted at the current density of 100 mA cm^{-2} (Fig. 2f). Pt-NPs@NPCNs–Co showed little change after the HER tests (Fig. S11, ESI†), indicating their stability. ICP-MS analysis (Table S3, ESI†) confirmed the absence of metal ions in the electrolyte after the HER tests.

Based on DFT calculations using atomic models of Pt (111) and Pt (111)-Co electrocatalysts (Fig. S12 and S13, ESI†), our investigation has revealed that electron transfer from Co to Pt through the skeleton results in the formation of an electron depletion region around Co-COP alongside an electron accumulation region around the Pt surface, as illustrated in Fig. 3a. This electron transfer process is responsible for promoting intermediate adsorption, thereby leading to a higher level of

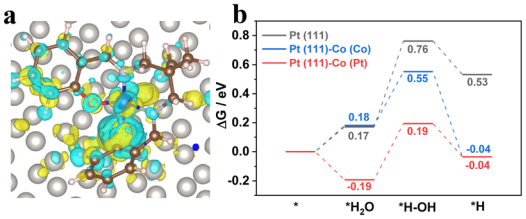

Fig. 3 (a) Charge-density difference plot of Pt (111)-Co. Atom color: C brown, Co blue, N violet, O red and Pt silver. Yellow and cyan iso-surface represents electron accumulation and electron depletion. (b) Energy profile of water dissociation on the Pt (111) (black), Pt (111)-Co (Co) (blue) and Pt (111)-Co (Pt) (red).

stability during the HER process. Our experimental findings have provided further insights indicating that water dissociation is the RDS for Pt-NPs@NPCNs, which is further accelerated by Co-COP, with both Pt and Co atoms competing for water adsorption. Fig. 3b shows that the theoretical Gibbs free energy to adsorb water on the Pt atoms in the Pt (111)-Co catalyst is exoergic (−0.19 eV, Pt (111)-Co (Pt)), which is less than that adsorbed on the Co atoms (0.18 eV, Pt (111)-Co (Co)) and Pt (111) (0.17 eV). Notably, the water dissociation energy barrier of Pt (111)-Co (Co) (0.37 eV) is lower than that of Pt (111)-Co (Pt) (0.38 eV) and Pt (111) (0.59 eV), but the activation energy of the Volmer step in Pt (111)-Co (Pt) (0.38 eV) is much lower than Pt (111)-Co (Co) (0.55 eV) and Pt (111) (0.76 eV). Therefore, the Co-COP primarily stems the electron structure of the Pt NPs and improves the water dissociation step of the electrocatalyst.

In summary, we present a novel bimetallic catalyst Pt-NPs@NPCNs–Co, with improved HER activity and stability. Its design involves a three-step process resulting in Pt NPs dispersed uniformly on the NPCNs–Co surface. This catalyst, in 1 M KOH solution, shows better performance than 20% Pt/C at low Pt loading, demonstrating enhanced efficiency through a synergistic interaction with Co. The study offers a path for designing more effective bimetallic catalysts for alkaline HER.

This work was supported by the National Key R&D Program of China (2022YFA1502902), the National Natural Science Foundation of China (22271218, 22071182, 22201209, and 21931007), and the Research Fund Program of Guangdong Provincial Key Laboratory of Fuel Cell Technology (FC202210).

Conflicts of interest

There are no conflicts to declare.

Notes and references

1 X. Wang, Y. Zheng, W. Sheng, Z. J. Xu, M. Jaroniec and S.-Z. Qiao, *Mater. Today*, 2020, **36**, 125.
2 C. Li and J. B. Baek, *ACS Omega*, 2020, **5**, 31.
3 J. Yan, Z. Xi, L. Cong, K. Lv, R. Xin, B. Cao, B. Liu, J. He and J. Zhang, *Small*, 2022, **18**, e2205603.
4 A. Shan, X. Teng, Y. Zhang, P. Zhang, Y. Xu, C. Liu, H. Li, H. Ye and R. Wang, *Nano Energy*, 2022, **94**, 106913.
5 T. Ma, H. Cao, S. Li, S. Cao, Z. Zhao, Z. Wu, R. Yan, C. Yang, Y. Wang, P. A. van Aken, L. Qiu, Y. G. Wang and C. Cheng, *Adv. Mater.*, 2022, **34**, e2206368.
6 J. Fan, Z. Feng, Y. Mu, X. Ge, D. Wang, L. Zhang, X. Zhao, W. Zhang, D. J. Singh, J. Ma, L. Zheng, W. Zheng and X. Cui, *J. Am. Chem. Soc.*, 2023, **145**, 5710.
7 J. Chen, M. Aliasgar, F. B. Zamudio, T. Zhang, Y. Zhao, X. Lian, L. Wen, H. Yang, W. Sun, S. M. Kozlov, W. Chen and L. Wang, *Nat. Commun.*, 2023, **14**, 1711.
8 S. Zhou, H. Jang, Q. Qin, L. Hou, M. G. Kim, S. Liu, X. Liu and J. Cho, *Angew. Chem., Int. Ed.*, 2022, **61**, e202212196.
9 K. L. Zhou, Z. Wang, C. B. Han, X. Ke, C. Wang, Y. Jin, Q. Zhang, J. Liu, H. Wang and H. Yan, *Nat. Commun.*, 2021, **12**, 3783.
10 L. Zhang, Y. Jia, H. Liu, L. Zhuang, X. Yan, C. Lang, X. Wang, D. Yang, K. Huang, S. Feng and X. Yao, *Angew. Chem., Int. Ed.*, 2019, **58**, 9404.
11 Y. Guo, B. Hou, X. Cui, X. Liu, X. Tong and N. Yang, *Adv. Energy Mater.*, 2022, **12**, 2201548.
12 K. Feng, J. Xu, Y. Chen, S. Li, Z. Kang and J. Zhong, *Adv. Sci.*, 2022, **9**, e2203199.
13 S. Zhu, X. Qin, F. Xiao, S. Yang, Y. Xu, Z. Tan, J. Li, J. Yan, Q. Chen, M. Chen and M. Shao, *Nat. Catal.*, 2021, **4**, 711.
14 R. Subbaraman, D. Tripkovic, D. Strmcnik, K.-C. Chang, M. Uchimura, A. P. Paulikas, V. Stamenkovic and N. M. Markovic, *Science*, 2011, **334**, 1256.
15 H. Tan, B. Tang, Y. Lu, Q. Ji, L. Lv, H. Duan, N. Li, Y. Wang, S. Feng, Z. Li, C. Wang, F. Hu, Z. Sun and W. Yan, *Nat. Commun.*, 2022, **13**, 2024.
16 A. Arora, P. Oswal, A. Datta and A. Kumar, *Coord. Chem. Rev.*, 2022, **459**, 214406.
17 H. M. Castro-Cruz and N. A. Macias-Ruvalcaba, *Coord. Chem. Rev.*, 2022, **458**, 214430.
18 S. An, X. Li, S. Shang, T. Xu, S. Yang, C. X. Cui, C. Peng, H. Liu, Q. Xu, Z. Jiang and J. Hu, *Angew. Chem., Int. Ed.*, 2023, **62**, e202218742.
19 S. Huang, K. Chen and T.-T. Li, *Coord. Chem. Rev.*, 2022, **464**, 214563.
20 D. Jiang, *Chemistry*, 2020, **6**, 2461.
21 C. Gu, N. Hosono, J.-J. Zheng, Y. Sato, S. Kusaka, S. Sakaki and S. Kitagawa, *Nature*, 2019, **363**, 387.
22 Y. Su, K. I. Otake, J. J. Zheng, S. Horike, S. Kitagawa and C. Gu, *Nature*, 2022, **611**, 289.
23 Y. Su, Z. Wang, A. Legrand, T. Aoyama, N. Ma, W. Wang, K. I. Otake, K. Urayama, S. Horike, S. Kitagawa, S. Furukawa and C. Gu, *J. Am. Chem. Soc.*, 2022, **144**, 6861.
24 H. Wu, Z. Chen, Y. Wang, E. Cao, F. Xiao, S. Chen, S. Du, Y. Wu and Z. Ren, *Energy Environ. Sci.*, 2019, **12**, 2697.
25 Z. Ma, H. Tian, G. Meng, L. Peng, Y. Chen, C. Chen, Z. Chang, X. Cui, L. Wang, W. Jiang and J. Shi, *Sci. China Mater.*, 2020, **63**, 2517.
26 B. Zhang, L. Chen, Z. Zhang, Q. Li, P. Khangale, D. Hildebrandt, X. Liu, Q. Feng and S. Qiao, *Adv. Sci.*, 2022, **9**, e2105912.
27 Y. Zhang, J. Yan, X. Ren, L. Pang, H. Chen and S. Liu, *Int. J. Hydrogen Energy*, 2017, **42**, 5472.
28 Y. Chen, J. Li, N. Wang, Y. Zhou, J. Zheng and W. Chu, *Chem. Eng. J.*, 2022, **448**, 137611.
29 F. Kong, X. Fan, X. Zhang, L. Wang, A. Kong and Y. Shan, *Carbon*, 2019, **149**, 471.
30 J. Bao, J. Wang, Y. Zhou, Y. Hu, Z. Zhang, T. Li, Y. Xue, C. Guo and Y. Zhang, *Catal. Sci. Technol.*, 2019, **9**, 4961.
31 Y. Wang, W. He, L. Wang, J. Yang, X. Xiang, B. Zhang and F. Li, *Chem. – Asian J.*, 2015, **10**, 1561.
32 S. Park, Y.-L. Lee, Y. Yoon, S. Y. Park, S. Yim, W. Song, S. Myung, K.-S. Lee, H. Chang, S. S. Lee and K.-S. An, *Appl. Catal., B*, 2022, **304**, 120989.
33 R. Andaveh, G. B. Darband, M. Maleki and A. S. Rouhaghdam, *J. Mater. Chem. A*, 2022, **10**, 5147.
34 S. Z. Dong, Y. S. Li, Z. L. Zhao, R. C. Li, J. Q. He, J. P. Yin, B. Yan and X. Zhang, *ChemistrySelect*, 2022, **7**, 20.
35 Y. L. Jia, Z. Q. Xue, Y. L. Li and G. Q. Li, *Energy Environ. Mater.*, 2022, **5**, 1048.
36 D. Cao, H. Xu, H. Li, C. Feng, J. Zeng and D. Cheng, *Nat. Commun.*, 2022, **13**, 5843.